Springer

Journal of Mechanical Science and Technology 23 (2009) 2366~2375

Journal of Mechanical Science and Technology

www.springerlink.com/content/1738-494x
DOI 10.1007/s12206-009-0626-7

CFD analysis of flow phenomena inside thermo vapor compressor influenced by operating conditions and converging duct angles †

Hyomin Jeong[3], Tony Utomo[2], Myoungkuk Ji[2], Yonghun Lee[2], Gyeonghwan Lee[1] and Hanshik Chung[3,*]

[1]*Graduate School of Department of Mechanical and Precision Engineering, Gyeongsang National University, 445 Inpyeong-dong, Tongyeong, Gyeongsangnamdo 650-160, Korea Korea*
[2]*Department of Mechanical and Precision Engineering, Gyeongsang National University, 445 Inpyeong-dong, Tongyeong, Gyeongsangnamdo 650-160, Korea*
[3]*Department of Mechanical and Precision Engineering, Institute of Marine Industry, Gyeongsang National University, 445 Inpyeong-dong, Tongyeong, Gyeongsangnamdo 650-160, Korea*

(Manuscript Received June 25, 2008; Revised May 6, 2009; Accepted May 12, 2009)

Abstract

A thermo vapor compressor is simply a steam ejector employed in a multi effect desalination process. A greater understanding of flow phenomena inside an ejector plays an important role in its performance improvement. In this paper, CFD investigation has been carried out to study the flow structure inside a steam ejector. This research revealed the influence of operating pressures and ejector geometries on the flow structure and the performance of a steam ejector. The CFD results were verified with available experimental data. The angle of the converging duct as the geometry parameter was varied as 0^o, 0.5^o, 1^o, 2^o, 3.5^o and 4.5^o. The best performance was obtained by the ejector with converging duct angle of 1^o.

Keywords: Thermo vapor compressor; Steam ejector; Performance; CFD; Desalination

1. Introduction

A thermo vapor compressor (TVC) is simply a steam ejector employed in the multi effect desalination (MED) system. It is an essential part in governing the total process of the MED system [1-3]. Hence, the accurate prediction of the TVC performance is needed to promote the reliability of the process. The enhancement of the TVC entraining efficiency improves the performance of MED significantly. Accordingly, a high efficiency TVC should be designed that can save motive steam and increase the amount of suction steam.

To improve the performance of ejector systems, an investigation of the flow inside the ejector is required. Flow visualization methods are useful to determine the different flow patterns occurring in ejectors [4], to study the pseudo-shock structure of supersonic jets [5] and to visualize the turbulent structures of the flow [6]. Desevaux (2001) proposed a method for visualizing the mixing zone between two co-axial flows in an ejector with laser tomography [7]. Nevertheless, successful visualizations have been obtained only for low values of the entrainment ratios (less than 0.3). For the higher suction flow rates (entrainment ratio more than 0.3), this method produced a poor quality of the flow visualizations and the mixing zone could not be identified accurately. This method obviously could not be used to visualize the flow phenomena inside the TVC that typically has entrainment ratio more than 0.3. Achieving this objective, computational fluid dynamics (CFD) technique

† This paper was recommended for publication in revised form by Associate Editor Gihun Son

*Corresponding author. Tel.: +82 55 640 3185, Fax.: +82 55 640 3188
E-mail address: hschung@gnu.ac.kr

can be applied reasonably.

Numerous CFD studies about supersonic ejectors and nozzles have been performed since the 1990s [8-11]. However, some very fundamental problems have yet to be overcome, especially the modeling of shock-mixing layer interaction or ejector operation at different conditions. Some of them did not consider compressibility [9] or turbulence [8].

In this paper, the effects of compressibility and turbulence are accommodated to study the flow phenomena inside a steam ejector by CFD technique. This research is focused on the influence of operating pressures and ejector geometries on the performance of a steam ejector.

An important parameter used to describe the performance of an ejector as TVC is 'an entrainment ratio':

$$ER = \frac{\dot{m}_s}{\dot{m}_m} \tag{1}$$

where $\dot{m}_s$ and $\dot{m}_m$ are mass flow rate for secondary fluid and motive fluid, respectively.

2. Steam ejector

The second part consisting of the paper body must be edited in double column format.

A steam ejector performs the mixing and recompression of two fluid streams (Fig. 1). The fluid with the highest total energy called primary or motive stream (stream 1 in Fig. 1), flows through a convergent divergent nozzle to reach supersonic velocity, creates the low pressure region at the nozzle exit. The secondary or suction stream (stream 2) is drawn into the flow by an entrainment-induced effect and then it is accelerated. Mixing and recompression of the resulting stream then occurs in a mixing chamber (converging duct and/or throat), where complex interactions occur between the mixing layer and shocks. In this occurrence, a mechanical energy is transferred from the highest to the lowest energy level, with a mixing pressure lying between the motive or driving pressure and the suction pressure.

Generally, steam ejectors can be classified into two categories according to the position of the nozzle [12]. For the ejector with its primary-nozzle exit located within the constant-area section, the mixing of the primary and the entrained flows occurs inside the constant-area section and the ejector is known as

Table 1. Ejector specifications.

Ejector Type	Specifications	Value
First Experiment (Pilot Plant)	Model	Constant pressure mixing ejector
	Overall length	2800 mm
	Body Material	Carbon Steel
	Primary Inlet D	52.7 mm
	Secondary Inlet D	195.9 mm
	Outlet D	202.7 mm
	Operating Fluid	Steam
Second Experiment (Pilot Plant)	Model	Constant pressure & area mixing ejector
	Overall length	5485.4 mm
	Body Material	Carbon Steel
	Primary Inlet D	80 mm
	Secondary Inlet D	404.4 mm
	Outlet D	436 mm
	Operating Fluid	Steam

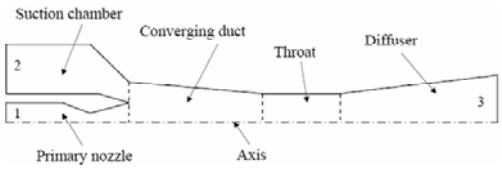

Fig. 1. Typical ejector geometry.

D_{throat} (mm)	D_{exit} (mm)	Area Ratio (A_{exit}/A_{throat})	Geometries
36.5	87.2	5.71	

Fig. 2. Ejector configurations.

"constant-area mixing ejector." For constant-pressure mixing ejector, the primary-nozzle exit is located within the converging-area section (converging duct). In this kind of ejector, it was assumed that the mixing of the primary and the entrained streams occurs in the converging duct with a uniform or constant pressure. The ejector used in these experiments has the general specifications and configuration as shown in Table 1 and Fig. 2.

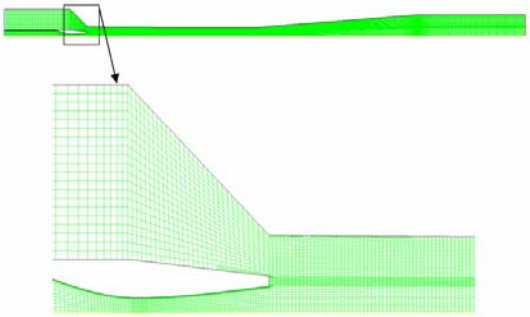

Fig. 3. 2D axisymmetric quadrilateral grid structure.

3. CFD modeling

3.1 Ejector model

The ejector was modeled as a 2D axisymmetric model in a commercial CFD software package (FLUENT). The grid structure was quadrilateral structured as shown in Fig. 3. The grid was initially made at about 24,000 elements and later adapted to about 30,000 elements to confirm that the results are grid independent. The grid density was concentrated on the areas where significant phenomena were expected.

In the CFD simulation process, suitable turbulence model also play an important part in order to get reasonably good results. Along with the grid refinement test, two different turbulence models were also tested in this research. The results are illustrated in Table 2.

From this table, it is observed that the entrainment ratio was insensitive neither to the grid number nor to the turbulence model. However, from the comparison to the experimental result, it is seen that standard k-ε with adapted grid produces the highest error. This error is based on the experimental data and the value is over than 10%, both from the coarse and fine grid. Conversely, the standard k-ε with original grid showed a better result compared to the previous one for both coarse and fine grid. In fact, they give the same result obtained from a realizable k-ε model with both adapted grid structure.

To investigate the flow phenomena and the influence of ejector geometries on its performance, variations of converging duct angle were made at 0.5^{o}, 1^{o}, 2^{o}, 3.5^{o} and 4.5^{o} for the constant-pressure mixing ejector. The constant-area mixing ejector is also investigated by setting the converging duct angle as 0^{o}.

Table 2. Comparison of CFD model to experimental results.

Original Cell Number	Turbulence Model	y^{+} Wall Treatment	Final Cell Number	ER from CFD Calculation	Error (%)
12,000	Standard k - ε	Non adaption	12,000	0.91	9.6
12,000	Standard k - ε	Adaption	24,000	0.93	12.0
12,000	Realizable k - ε	Adaption	24,000	0.91	9.6
24,000	Standard k - ε	Non adaption	24,000	0.91	9.6
24,000	Standard k - ε	Adaption	30,000	0.92	10.8
24,000	Realizable k - ε	Adaption	30,000	0.91	9.6

The entrainment ratio obtained from experimental is 0.83

3.2 Governing equations

Modeling ejector flow is based on the conservation equations; namely, the continuity, momentum, and energy equation. Because of the nature of flow in the ejector, those equations need to be written in the compressible, steady state, axisymmetric form. For variable density flows, the Favre averaged Navier-Stokes equations are the most suitable. The governing equations refer to the commercial code. (FLUENT)

Although a steady state is desired, the unsteady term is conserved since from a numerical point of view, governing equations are solved with a time marching technique. The discretized system was solved by using the "coupled-implicit" solver.

3.3 Turbulence modeling

High speed flow and extensive mixing occur in the ejector. This makes the flow highly turbulent and this turbulent mixing is the dominant entrainment mechanism in the ejector. The realizable k-ε model is employed to govern the turbulence characteristics in this work. This turbulence model was proposed by Shih et al. [13]. The term "realizable" means that the model satisfies certain mathematical constraints on Reynolds stress, consistent with the physics of turbulent flows. An immediate benefit of this model is that it more accurately predicts the spreading rate of both planar and round jets.

In addition, standard wall functions are considered. Special care is given to the near wall grid, by a local

adaptation following $30 \le y^+ \le 50$.

The density of the saturated steam is evaluated using the ideal gas relation as part of the calculation as it progresses. Other properties are defined as constant throughout the simulation.

3.4 Fluid properties

Saturated steam is used as the working fluid of the model by employing the assumption of an ideal gas. Even though the ideal gas relation seemed to be the unrealistic assumption to the model, for the ejector application where the operating pressure is relatively low, it was proved by some researchers that it provided similar results to a real gas model [14]. The properties of saturated steam are as shown in Table 3.

3.5 Boundary conditions

Boundary conditions were set as pressure-inlet for two faces entering a primary nozzle and ejector. Pressure-outlet boundary was set for the one leaving ejector. These parameters were varied during the simulation.

The variations of motive pressure at pressure-inlet boundary are 2.66, 3 and 3.5 bar. The suction pressures are varied between 0.13, 0.16 and 0.19 bar. At the pressure-outlet boundary, the discharge pressure was varied from 0.2 bar to 0.31 bar. The values of each boundary were assigned as the saturation properties (temperature and pressure) of each operating state. There was no difference between an input of the stagnation pressure and static pressure considering that the velocity of the flow entering and leaving the domain was thought to be relatively small compared with the supersonic speed during the flow process of the ejector A motive and suction side applied the pressure condition that they define the turbulence intensity as 5% and the wall applied the standard wall function, that is, the no-slip condition.

Table 3. Properties of saturated steam.

Property	Value
Density	Ideal Gas Model
Cp (Specific Heat)	2170 J/kg^{o}K
Conductivity	0.0276 W/m^{o}K
Viscosity	1.31619 x 10^{-5} kg/ms
Molecular Weight	18.015 kg/mol ^{o}K

4. Results and discussion

The calculations were considered as converged when the following two converging criteria were met. First, every type of the calculation residual must be reduced [to] lower than the specified value (less than 10^{-6}). Second, the calculated mass fluxes of every face of the model were stable. In addition, the converged solutions have to satisfy the principle of conservation of mass. The difference between the summation of mass fluxes entering and leaving the model should not be greater than 10^{-4} kg.s^{-1}.

4.1 The effect of operating pressures

Fig. 4 shows the Mach number and static pressure distribution in the ejector from the inlet of the converging duct to the exit of the subsonic diffuser. It can be seen at the nozzle exit plane that the supersonic primary stream leaves the primary nozzle with its static pressure greater than that in the mixing chamber. Accordingly, it is capable of additional expansion and acceleration as an "*under-expanded*" wave with some value of the "*expansion angle.*" The first series of oblique shock and expansion waves, called the "*diamond wave*" pattern, is induced to maintain the static pressure across the free boundary between the primary jet core and the surrounded fluid,. The region where the series of shock waves occurs is called the shock train region. This phenomenon creates the fluctuation of static pressure at the center line of the ejector while the flow passes through a mixing tube (Fig. 4(b)). The shock train phenomenon obtained in this CFD investigation is conformable to that of laser tomography obtained from experiment of Desevaux (2001).

The occurrence of a diamond wave jet core in the mixing tube indicates the semi-separation between the high speed primary flow and the surrounding secondary fluid. The shear stress layer interfacing between them is presented because of the large velocity difference between these two streams. The shear mixing of two streams begins when the secondary fluid is entrained and interfaces with the expanded wave. This shear mixing process causes the secondary fluid to accelerate flowing through the converging duct. Conversely, the shear mixing and the viscosity of the fluid cause the diamond wave to decay. As investigated in Fig. 4(b), the static pressure of the flow has a steady decrease at the beginning of the flow process, and the

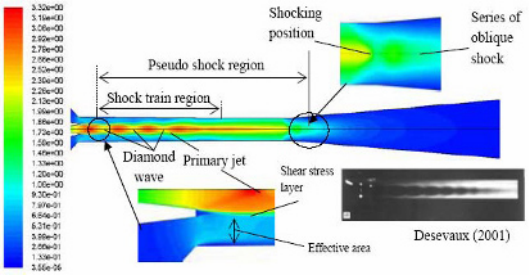

(a) Contour of Mach number.

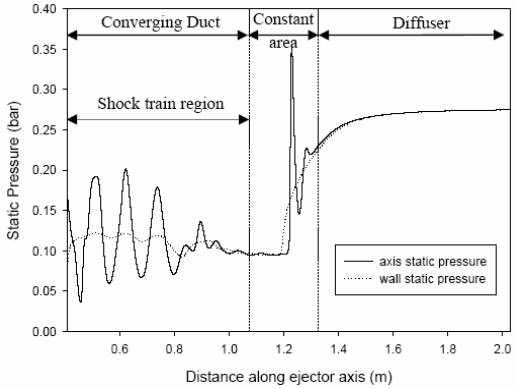

(b) Static pressure distribution.

Fig. 4. Mach number and static pressure distribution inside the steam ejector.

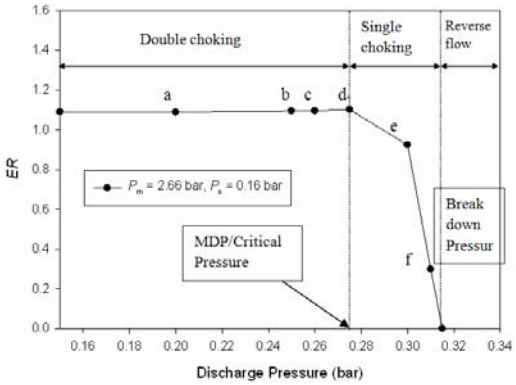

Fig. 5. The effect of discharge pressure on the ejector performance.

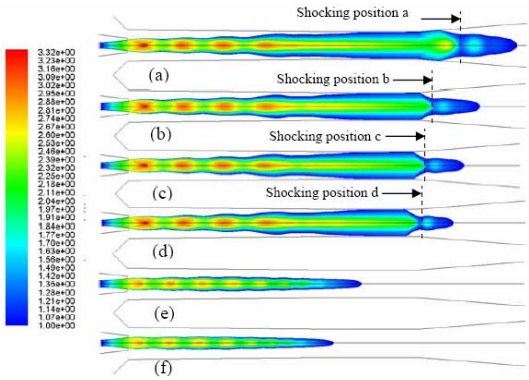

Fig. 6. Contour of Mach number for various discharge pressures; (a) P_d = 0.2 bar, (b) P_d = 0.25 bar, (c) P_d = 0.26 bar, (d) P_d = 0.275 bar, (e) P_d = 0.3 bar, and (f) P_d = 0.31 bar.

intensity of the diamond wave is reduced.

Most of the entrained secondary fluid accelerates and reaches sonic velocity at the throat of the mixing tube. Very small amounts of them move slightly faster than the sonic value when it flows close to the shear stress layer, but slower when it flows close to the wall boundary layer. Moreover, it is seen that the intensity of the diamond wave reduces when the primary jet core runs with lower supersonic speed resulting in a relatively smooth jet core. Hence, the secondary flow can be considered as choked. The choke area or "*Effective area*" of the secondary fluid can be estimated from the annulus area between the wall of an ejector throat and the primary fluid jet core. During the choke flow mode, the entrainment ratios remained constant.

At a certain distance into the ejector throat or in the beginning of the diffuser section, called the "*Shocking position,*" a non-uniform stream produces the second series of oblique shock waves. Accordingly, the static pressure recovers gradually to discharge value and the flow speed decreases gradually to subsonic level as it passes through the diffuser. This phenomenon is described in Fig. 4(b). Across this process, the mixed stream loses most of its total pressure.

The operating modes of ejector are divided into the double choking, single choking and reverse flow modes by the changes of discharge pressures. In the double choking range, the entrainment ratio remains constant and stable below the maximum discharge pressure (MDP) and the choked motive steam in the nozzle mixes the suction stream and passes the converging/diverging duct. At the discharge pressure over the MDP, the entrainment ratio decreases sharply. The sudden drop of entrainment ratio indicates the ejector operates in the single choking mode (Fig. 5).

Fig. 6 shows the Mach contour at different discharge pressures, while the motive and suction pressure remain constant at 2.66 bar and 0.16 bar, respectively. This figure illustrates the changing of flow structure, represented by Mach contour, affected by

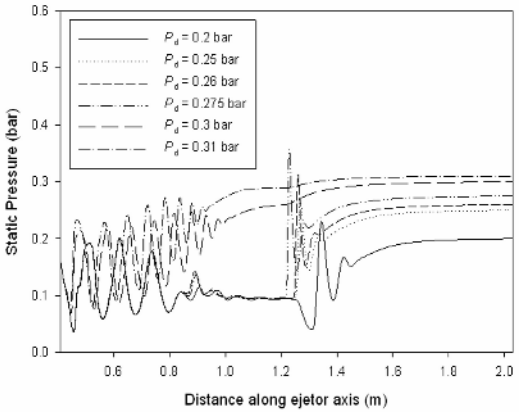

Fig. 7. The effect of discharge pressure on static pressure distributions along the center line of the ejector.

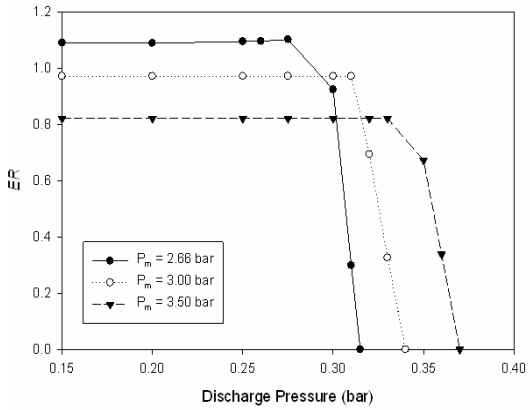

Fig. 8. The effect of operating pressure on the ejector performance for various motive pressures.

discharge pressure as plotted in Fig. 5. Increasing discharge pressure causes the shocking position to move upstream into the ejector throat. However, when the back pressure does not exceed the critical point or within the double choked flow region (a, b, c and d), the shock will not affect the mixing behavior of the two streams. Moreover, flow structures in front of a shocking position are shown unchanged and the size of the primary jet core remains constant and independent from downstream conditions. It is thought, that during this choke flow region, the effective areas are always forced to appear within the constant area throat, since, the entrainment ratio remained constant.

When the discharge pressure is increased to higher than the critical point (e and f), the second series of oblique shocks is forced to move further upstream and combine with the first series of oblique shocks to form a single series of oblique shocks. This movement of the second series of oblique shocks causes the secondary fluid to be no longer choked, hence, disturbing the entrainment process. It can be investigated from the low-entering of an entrained fluid speed and hence, the increasing of static pressure before shock (Fig. 7).

Fig. 8 shows the effect of discharge pressure (P_d) on the entrainment ratio at various motive pressures (P_m) at constant suction pressure (P_s). The entrainment ratio decreases inversely to the increase of motive pressure. This phenomenon could be explained by the fact that the increase of motive pressure will affect the increase of nozzle exit pressure. While the suction pressure remains constant, the increase of motive pressure results in the decrease of pressure difference between suction and nozzle exit. Obviously, a lower pressure difference between suction and nozzle exit (mixing chamber) would yield a less-entrained flow rate from the secondary suction inlet. Therefore, entrainment ratio would decrease as the primary-flow pressure increases.

On the other hand, a larger motive pressure would push the oblique shock wave occurring in the diffuser section more downstream, thus increasing the shock intensity. Consequently, the critical discharge pressure is increased by increasing motive pressure. Fig. 9 illustrates the Mach contour for various motive pressures at constant suction and discharge pressure of 0.16 bar and 0.275 bar, respectively. The increase of motive pressure results in the increase of mass flow through primary nozzle and the momentum of the flow. The increasing of momentum allowed the primary fluid to leave and further under-expand and accelerate with larger expansion angle. It causes the diamond flow to shock at a higher Mach number at the first oblique shock as can be seen in Fig. 10. The increased expansion angle causes the enlarging of a jet core; therefore, the annulus effective area is reduced and less secondary fluid can be entrained and accelerated through the steeper converging duct. However, with higher momentum of the jet core, the shocking position moves downstream and the ejector can be operated at a higher discharged pressure.

Fig. 11 presents the entrainment ratio as a function of the discharge pressure at three different values of P_s and constant P_m = 2.66 bar. An increase in P_s always causes an increase in the driving pressure difference between suction and nozzle exit pressure and thereby increases the entrainment ratio. Furthermore, increasing the suction pressure increases the critical

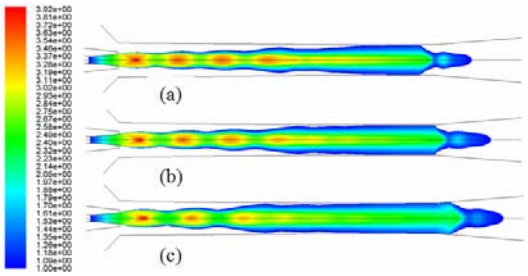

Fig. 9. Contour of Mach number for various motive pressures; (a) P_m = 2.66 bar, (b) P_m = 3.0 bar, and (c) P_m = 3.5 bar.

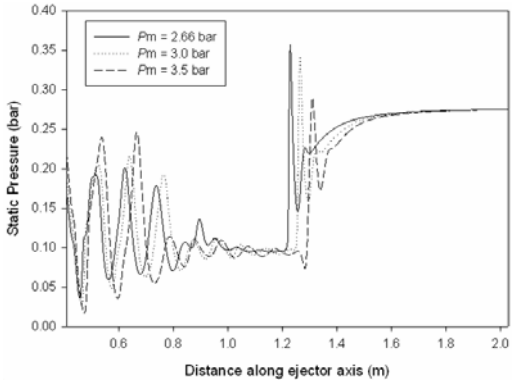

Fig. 10. The effect of primary fluid pressure on static pressure distributions along the centerline of the ejector.

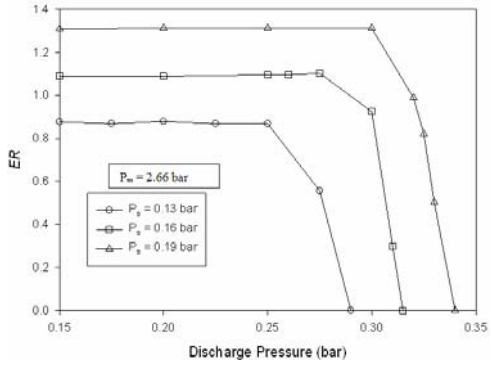

Fig. 11. The effect of operating pressure on the entrainment ratio at various suction pressures.

discharge pressure.

Fig. 12 illustrates the contour of Mach number for various suction pressures. It can be seen that the expansion angle of the under-expanded wave is influenced by an increasing of the secondary fluid pressure. The pressurized condition causes the lowering of expansion angle, thus resulting in smaller jet core and larger effective area. The expanded wave is further accelerated at a lower Mach number. Therefore, the

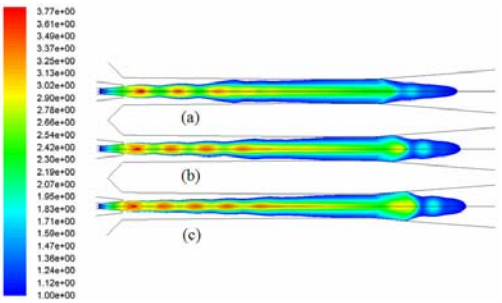

Fig. 12. Contour of Mach number for various suction pressure; (a) P_s = 0.13 bar, (b) P_s = 0.16 bar, (c) P_s = 0.19 bar.

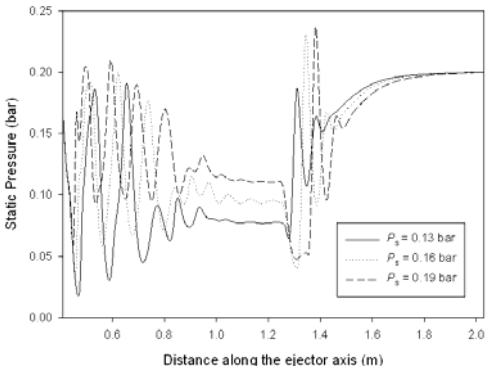

Fig. 13. The effect of suction pressure on static pressure distribution along the center line of the ejector.

momentum of the jet core is reduced. However, an enlarged effective area allows a larger amount of secondary fluid to be entrained and pass through the converging duct. Total momentum of the mixed stream, which is decreased by the jet core, is compensated by the higher secondary fluid pressure. It can be concluded that the total momentum of the mixed stream becomes higher and the shocking position moves downstream as the secondary fluid pressure rises. This enables the ejector to be operated at higher discharge pressure. The static pressure distribution along the center line of the ejector is illustrated in Fig. 13. The shocking position is shifted at more downstream as the secondary fluid pressure increased. Furthermore, the increasing of suction pressure affects the higher pressure on the series of oblique shock.

4.2 The effect of converging duct angle

The simulation is conducted at constant primary and discharge pressure at 2.66 bar and 0.25 bar, respectively. The suction pressures are varied at 0.13, 0.16 and 0.19 bar.

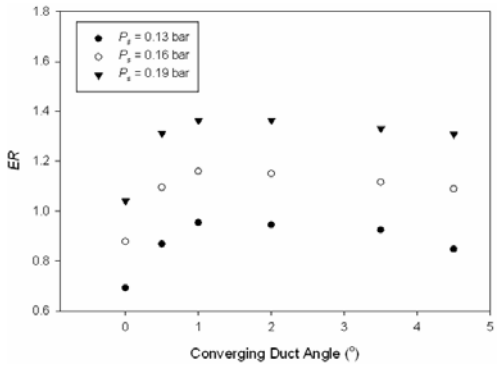

Fig. 14. The effect of converging duct angle on the entrainment ratio.

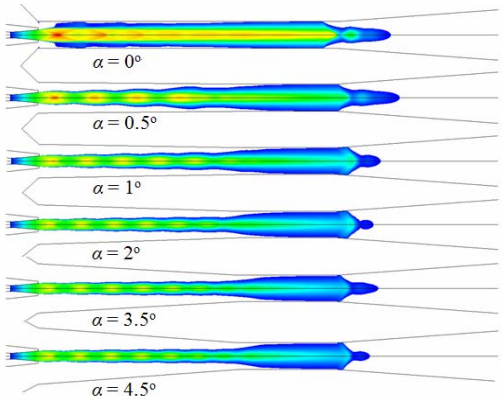

Fig. 15. Effect of converging duct angle on the contour of Mach number.

Fig. 14 and Fig. 15 demonstrate the influence of converging duct angle on the entrainment ratio and contours of Mach number of the ejector, respectively. It is seen that the trend lines for different suction pressures are similar. The entrainment ratio increases sharply from constant-area mixing ejector ($\alpha = 0^{o}$) to constant-pressure mixing ejector at $\alpha = 0.5^{o}$. Concerning the flow structure, the constant-area mixing ejector is apparently different from the converging duct mixing (constant-pressure mixing) ejector.

The effect from the converging duct inlet is obvious. Less shear mixing and viscous effect in the converging duct causes the expanded wave to leave the nozzle with a large expansion angle. The result is a very large primary jet core and, consequently, a very small converging duct. For these reasons, smaller amounts of the secondary fluid can be entrained through this converging duct, and lessen the ejector entrainment ratio. Since the flow structures inside the constant-area mixing ejector are quite different from

Table 4. Experimental data sheet.

Operating condition		TVC PERFORMANCE DATA			
Duct angle: α	Pressure (bara)	Motive steam flow	Expansion ratio	Compression ratio	Suction rate
0	3.5	2.04	42.78	2.94	0.31
	3.2	1.87	37.59	2.84	0.35
	2.7	1.59	33.49	2.86	0.45
	2.2	1.30	25.36	2.72	0.31
	2.0	1.19	33.11	3.44	0.30
0.5	3.5	2.04	34.50	2.60	0.41
	2.7	1.59	24.91	2.52	0.54
	1.8	1.05	30.44	3.62	0.33
1.0	3.5	2.04	41.08	2.76	0.54
	3.3	1.93	38.56	2.77	0.56
	3.0	1.76	36.96	2.98	0.56
	2.7	1.59	30.60	2.89	0.64
	2.4	1.42	37.09	3.42	0.53
	2.2	1.30	33.30	3.17	0.58
	2.0	1.19	50.06	4.66	0.40
	1.8	1.05	61.43	6.32	0.36

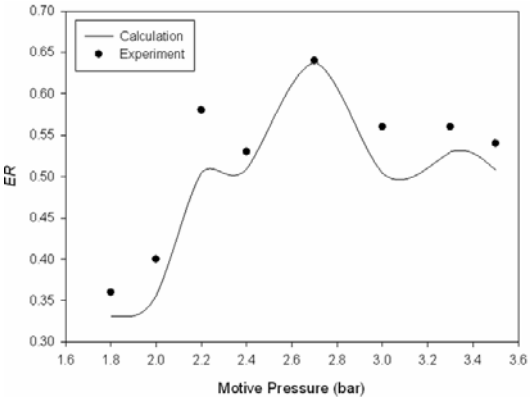

Fig. 16. The entrainment ratio of ejector with α = 1° at various motive pressure; P_m = 2.66 bar.

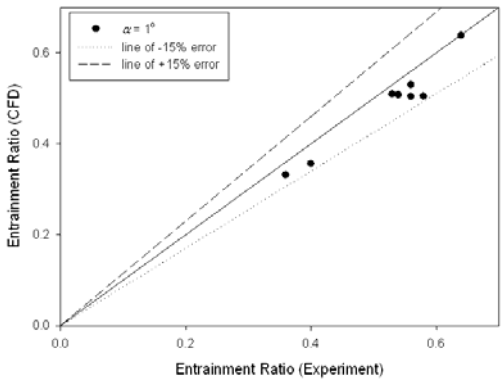

Fig. 17. Comparison of entrainment ratio between CFD and experimental results; P_m = 2.66 bar.

those of the converging duct mixing ejector, the position of the effective area is moved. Thus, the prediction of the trend of critical discharge pressure cannot be based only on the comparison of shocking position between these two ejectors. On the other hand, for the converging duct mixing ejector, the entrainment ratio is slightly increased when the angle varies from $\alpha = 0.5^{o}$ to $\alpha = 1^{o}$. Further increase in converging duct angle beyond $\alpha = 1^{o}$ results in a decrease of entrainment ratio. These slight differences in the entrainment ratio can be explained by the flow structures. The primary jet core of the smaller entrance ejector flows with slightly greater speed and hence higher momentum.

Entraining the secondary fluid under a higher effect of the shear mixing and the viscosity of the fluid on the expanded wave introduces the higher total pressure loss to the mixed stream. Therefore, the ejector with $\alpha = 0.5^{o}$ entrains lower secondary fluid. However, the benefit of increasing the converging duct angle is restricted to the fact that it also causes an increase of nozzle exit pressure, consequently decreasing the driving pressure of the suctioned fluid. For this reason, the entrainment ratio decreases contrary by further increase of converging duct angle beyond $\alpha = 1^{o}$.

For validation purposes, the CFD codes in this study are applied to simulate the real ejector and compare to the experimental data. The comparison is conducted for the ejector with converging duct angle $\alpha = 1^{o}$. The results are shown in Figs. 16 and 17. The discrepancies are less than 15%; therefore, the CFD results have a good agreement with experimental data. Experimental data is shown Table 4.

5. Conclusions

The effects of various operating pressures on the ejector performance have been investigated. Ejector shapes or geometries, i.e., converging duct angle, are also varied and the ejector performance is simulated. The converging duct angle $\alpha = 1^{o}$ gives the highest entrainment ratio. The CFD results have been validated with experimental results and they show a good agreement. The CFD visualization becomes a great benefit in the study because it can reveal the phenomena inside the ejector in detail. In all, the view points on ejector performance related to its flow structure can be understood precisely and it may be a very powerful tool to design an appropriate ejector for a particular case.

Acknowledgment

This research was financially supported by the Ministry of Education Science Technology (MEST) and Korea Industrial Technology Foundation (KOTEF) through the Human Resource Training Project for Regional Innovation and Second-Phase of BK 21 Project Korea.

Nomenclature

d : Discharge
ER : Entrainment ratio
m : Motive
$\dot{m}$: Mass flow rate (kg/s)
P : Pressure (bar)
s : Suction
α : Converging duct angle (^{o})

References

[1] M. A. Darwish and H. T. Ed-Dessouky, The heat recovery thermal vapor-compression desalting system: A comparison with other thermal desalination processes, *Applied Thermal Engineering*, 18 (1996) 523-537.

[2] Hamed, A. M. Zamamiri, S. Aly and N. Lior, Thermal performance and exergy analysis of thermal vapor compression desalination systems, *Energy Conversion Management*, 37 (1996) 379-387.

[3] N. M. Al-Najem, M. A. Darwish and F. A. Youssef, Thermo-vapor compression desalination: energy and availability analysis of single and multi-effect systems, *Desalination* 110 (1997) 223-238.

[4] J. Fabri and R. Siestrunck, Supersonic air ejectors, *Advances in Applied Mechanics*, 5 (1958) 1-34.

[5] K. Matsuo, Y. Miyazato and H. D. Kim, Shock train and pseudo-shock phenomena in internal gas flows, *Progress in Aerospace Science*, 35 (1999) 33-100.

[6] P. Desevaux, J. P. Prenel and G. Hostache, Flow visualization methods for investigating an induced flow ejector, *Flow Visualization Image Process*, 2 (1995) 61-74.

[7] P. Desevaux, A method for visualizing the mixing zone between two co-axial flows in an ejector, *Optics and Lasers in Engineering*, 35 (2001) 317-323.

[8] F. Chen, C. F. Liu and J. Y. Yang, Supersonic flow in the second-throat ejector-diffuser system, *Journal Spacecraft Rocket*, 31 (1) (1994) 123-129.

[9] S. B. Riffat, G. Gan and S. Smith, Computational

fluid dynamics applied to ejector heat pumps, *Applied Thermal Engineering*, 16 (4) (1996) 291-297.

[10] Rusly, E. Aye, Lu, Charters, W. W. S. and A. Ooi, CFD analysis of ejector in a combined ejector cooling system, *International Journal of Refrigeration*, 28 (2005) 1092-1101.

[11] S. D. Kim, I. S. Jeong and D. J. Song, A Computational Analysis of Unsteady Transonic/Supersonic Flows Over Backward Facing Step in Air Jet Nozzle, *Journal of Mechanical Science and Technology*, 21 (2) (2007) 336-347.

[12] D. W. Sun and I. W. Eames, Recent development in the design theories and applications of ejector-a review, *Journal Institute Energy*, 68 (1995) 65-79.

[13] T. H. Shih, W. W. Liou, A. Shabbir and J. Zhu, A new k-ε Eddy-Viscosity Model for high Reynolds number turbulent flows – Model development and validation, *Computer Fluids*, 24 (3) (1995) 227-238.

[14] T. Sriveerakul, S. Aphornratana and K. Chunnanond, Performance prediction of steam ejector using computational fluid dynamics: Part 1. Validation of the CFD results, *International Journal of Thermal Sciences*, 46 (2007) 812-822.

Hyo-Min Jeong received his Ph.D. degree from the University of Tokyo, Japan in 1992. Dr. Jeong is currently a Professor at the Department of Mechanical and Precision Engineering at Gyeongsang National University in Tongyeong, Korea. His research interests include Fluid Engineering, CFD, Cryogenic system, Ejector system, Mechanical Vapor Compression, and Cascade Refrigeration system.

Han-Shik Chung received his Ph.D. degree from Donga University, Korea in 1987. Dr. Chung is currently a Professor at the Department of Mechanical and Precision Engineering at Gyeongsang National University in Tongyeong, Korea. His research interests include Thermal Engineering, Heat Transfer, LNG Vaporizer Optimum, Solar Cell, and Fresh Water System from Sea Water.